Published in final edited form as:
Nature. 2010 April 1; 464(7289): 728–732. doi:10.1038/nature08893.

N-Myristoyltransferase inhibitors as new leads to treat sleeping sickness

Julie A. Frearson[1], **Stephen Brand**[1], **Stuart P. McElroy**[1], **Laura A.T. Cleghorn**[1], **Ondrej Smid**[1], **Laste Stojanovski**[1], **Helen P. Price**[4], **M. Lucia S. Guther**[1], **Leah S. Torrie**[1], **David A. Robinson**[1], **Irene Hallyburton**[1], **Chidochangu P. Mpamhanga**[1], **James A. Brannigan**[3], **Anthony J. Wilkinson**[3], **Michael Hodgkinson**[4], **Raymond Hui**[5], **Wei Qiu**[5], **Olawale G. Raimi**[2], **Daan M. F. van Aalten**[2], **Ruth Brenk**[1], **Ian H. Gilbert**[1], **Kevin D. Read**[1], **Alan H. Fairlamb**[1], **Michael A. J. Ferguson**[1], **Deborah F. Smith**[4], and **Paul G. Wyatt**[1]

[1]Drug Discovery Unit, Division of Biological Chemistry and Drug Discovery, College of Life Sciences, University of Dundee, Dundee, DD1 5EH, UK

[2]Division of Molecular Microbiology, College of Life Sciences, University of Dundee, Dundee, DD1 5EH, UK

[3]Structural Biology Laboratory, Department of Chemistry University of York, Heslington, York YO10 5YW, UK

[4]Centre for Immunology and Infection, Department of Biology and Hull York Medical School, University of York, Heslington, York YO10 5YW, UK

[5]Structural Genomics Consortium, University of Toronto, MaRS South Tower, 7th Floor, 101 College St, Toronto, Ontario, Canada M5G 1L7

Abstract

African sleeping sickness or human African trypanosomiasis (HAT), caused by *Trypanosoma brucei spp.*, is responsible for ~30,000 deaths each year. Available treatments for this neglected disease are poor, with unacceptable efficacy and safety profiles, particularly in the late stage of the disease, when the parasite has infected the central nervous system. Here, we report the validation of a molecular target and discovery of associated lead compounds with potential to address this unmet need. Inhibition of this target, *T. brucei N*-myristoyltransferase (*Tb*NMT), leads to rapid killing of trypanosomes both *in vitro* and *in vivo* and cures trypanosomiasis in mice. These high affinity inhibitors bind into the peptide substrate pocket of the enzyme and inhibit protein *N*-myristoylation in trypanosomes. The compounds identified have very promising pharmaceutical properties and represent an exciting opportunity to develop oral drugs to treat this devastating disease. Our studies validate *Tb*NMT as a promising therapeutic target for HAT.

Correspondence and request for materials should be addressed to P.G.W. (pgwyatt@dundee.ac.uk)..

Author Contributions The project management team responsible for experimental design and coordination of research activities at the University of Dundee comprised S.B., R.B., A.H.F., M.A.J.F., J.A.F., I.H.G., K.D.R., D.M.F.vA and P.G.W. and D.F.S. at the University of York. J.A.B., M.H. and A.J.W. optimized expression and produced the active *Tb*NMT used for screening in the Drug Discovery Unit. Biological studies were carried out by S.P.M., O.S, L.S.T, M.L.S.G., I.H., H.P.P. and chemical syntheses by L.C. and S.B.; structural biology and modelling by D.A.R., O.G.R. and C.P.M. at Dundee and R.H. and W.Q. at University of Toronto; and pharmacological studies by L.S.

Author Information Atomic coordinates and structure factors for the crystal structures have been deposited with the Protein Data Bank under accession codes 3H5Z and 2WSA for *Lm*NMT with bound myristoyl CoA and DDD85646, respectively. A patent relating to this work has been filed (PCT/GB2009/002084).

Supplementary Information is linked to the online version of the paper at www.nature.com/nature.

The authors declare no competing financial interests.

Europe PMC Funders Author Manuscripts

Protein *N*-myristoylation is a ubiquitous eukaryotic co- and post-translational modification and is required for membrane targeting and biological activity of many important proteins 1,2. The *N*-myristoylation reaction, *i.e.*, the transfer of $C_{14:0}$ myristic acid from myristoyl-coenzyme A (CoA) to the amino group of *N*-terminal glycine residues within specific sequence contexts 3, is catalysed by the enzyme myristoyl-CoA: protein *N*-myristoyltransferase (NMT; EC 2.3.1.97) 4. In *T. brucei*, NMT activity is encoded by a single gene, which has been shown to be essential for parasite growth using RNA interference 5. The effects of NMT knockdown on *T. brucei* are likely to be complex since more than 60 proteins are predicted to be *N*-myristoylated in this organism 6. Experimentally validated targets for NMT include ADP ribosylation factors (Arf) 7, ADP ribosylation-like factors (Arl) 8, a calpain-type protease (CAP5.5, *Tb*CALP1) 9 and, in the related *Leishmania major* and *T. cruzi* parasites, hydrophilic acylated surface proteins (HASPs) 10 and flagellar calcium-binding protein 11, respectively. The predicted pleiotropic effects of NMT inhibition on trypanosome physiology make it an attractive target for therapeutic intervention. NMT has also been considered as an anti-cancer 12, fungal 13 and viral 14 target. Fungal NMT orthologues have been shown to be druggable, although broad-spectrum activity has not been achieved. Nevertheless, since there is good evidence from these programmes that selectivity versus human NMT is possible, NMT has been proposed as a target for the treatment of human African trypanosomiasis (HAT) and other parasitic diseases 15,16. There are 2 human isozymes sharing 77% identity (*hu*NMT1 and 2) 17 of which *hu*NMT2 is the closest human homologue to *Tb*NMT, with overall 55% identity and 69% similarity. Based upon 31 residues that are within 5Å of DDD85646 in the active site, this rises to 83% identity and 90% similarity.

Pyrazole sulfonamide inhibitors of *Tb*NMT

To date, no drug-like, potent inhibitors of *Tb*NMT have been reported 18. Screening of a 62,000 diversity-based compound library 19 against *Tb*NMT identified a number of “lead-like” hits, including a chemically tractable series with moderate potency (2 μM) based on a pyrazole sulfonamide scaffold (DDD64558). Optimisation of the screening hit, involving the design and synthesis of over 200 compounds, identified highly potent inhibitors of *Tb*NMT with single digit nanomolar IC_{50} values and levels of selectivity over human NMT enzymes in the 1 to >100-fold range (Fig.1a). The relative lack of activity of the piperidine analogue (DDD85635) of DDD85602 indicated the terminal basic nitrogen of DDD85602 was crucial for activity. The series was optimised by rigidifying the flexible linker to the amine moiety of DDD85602 and by adding the chlorines observed to give an increase in activity in the unelaborated template (DDD73234). *Tb*NMT inhibitors so obtained (e.g. DDD85646) inhibited the proliferation of bloodstream form (BSF) *T. brucei* in culture with the best compounds yielding EC_{50} values between 0.8 and 3 nM and clear windows of selectivity (>200-fold) with respect to proliferation of a prototypical mammalian cell type (MRC5). We attribute the increased selectivity at the cellular level to differences in cell biology between host and parasite, although differential cellular pharmacokinetic behaviour has not been definitively ruled out. Critically, a tight correlation ($R^2 = 0.875$) was observed between IC_{50} and EC_{50} values for *Tb*NMT and *T. brucei* proliferation, respectively, over a 10,000-fold potency range (Fig. 1b); indicating that inhibition of *Tb*NMT was driving the observed anti-parasitic effect of these compounds. The poorer correlation for the most potent compounds (see lower left quadrant of Fig. 1b) is most likely due to the limit of the enzyme assay to provide accurate IC_{50} determinations for such highly active, tight-binding inhibitors (see Supplementary Information, Figure 1). As a result of its impressive potency in inhibiting both *Tb*NMT and *T. brucei* proliferation *in vitro*, together with its promising physicochemical properties, DDD85646 was assessed for efficacy in animal models of trypanosomiasis.

*Tb*NMT inhibitor cures acute HAT *in vivo*

DDD85646 is moderately bioavailable (ca. 20%) and demonstrates good exposure after oral dosing at 10 and 50 mg kg^{-1} to female NMRI mice, with the free drug level above the EC_{99} for *T. b. brucei* proliferation for over 6 and 10 h, respectively (Fig. 2a). Furthermore, this compound cured all animals in the *T. b. brucei* acute mouse model of HAT at a minimal oral dose of 12.5 mg kg^{-1} (b.i.d. for 4 days) (Fig 2b). Cure of all animals was also obtained with shorter oral dosing schedules: 100 mg kg^{-1} b.i.d. for one day and 25 mg kg^{-1} b.i.d. for 2 days. Importantly, DDD85646 also cured all animals at 50 mg kg^{-1} (b.i.d. for 2 days) in the more refractory, but clinically relevant *T. b. rhodesiense* model of HAT (see Supplementary Information, Figure 2). This reduced sensitivity *in vivo* is not due to reduced sensitivity to the compound *in vitro* (*T. b. rhodesiense* EC_{50} 0.6nM), but maybe a result of the known precedent for this species to occupy privileged sites *in vivo*. Notably, the efficacy observed for DDD85646 was comparable with the responses observed for the clinically-used drugs pentamidine and melarsoprol in the *T. b. brucei* model (minimal full cure doses were 1 mg kg^{-1} and 0.5 mg kg^{-1} (IP) respectively). Furthermore, despite the minimal window of *in vitro* enzyme selectivity between *Tb*NMT and mammalian (human) NMT (Fig. 1a and *vide infra*), this compound was well tolerated at efficacious doses.

*Tb*NMT inhibitors are trypanocidal

Addition of DDD85646 resulted in rapid killing of trypanosomes both *in vivo* and *in vitro* (Fig. 3a, b). Parasite counts dropped to below detectable levels within 12 h of dosing mice at 50 mg kg^{-1} b.i.d. Addition of compound (50 nM) to BSF *T. brucei* cultures *in vitro* also resulted in rapid killing with numbers of motile cells reduced to below detectable levels between 24 and 48 h. The apparent differences in kinetics of death between the *in vivo* and *in vitro* systems are most likely a combination of the harsher *in vivo* environment for drug-damaged trypanosomes and the fact that compound exposure reached higher concentrations *in vivo* (up to ~1 μM), compared with 50 nM *in vitro*.

The trypanocidal mechanism of compound action was confirmed by subjecting *T. brucei* treated *in vitro* with 50 nM compound to live/dead FACS analysis, which showed >95% cell death within 24 h of treatment (see Supplementary Information, Figure 3). Furthermore, wash-out experiments showed that death was irreversible after 48 h of exposure to 50 nM compound (data not shown). Microscopic examination of the trypanosomes treated with DDD85646 *in vivo* and *in vitro* revealed the same abnormal morphology, *i.e.*, the development of a large vesicular structure (Figure 3c). A scanning electron micrograph of a compound-treated trypanosome clearly shows the rounded and swollen features of this phenotype compared to control (Fig. 3d). Interestingly, rapid cell killing with a similar morphological phenotype has been observed previously following treatment with myristate analogues, such as 10-(propoxy)decanoic acid 20. This morphology closely resembles the ‘BigEye’ phenotype observed in BSF *T. brucei* when endocytosis is disrupted through the knockdown of clathrin heavy chain, *Tb*Rab5 21,22 or *Tb*Arf1 7 leading to expansion of the flagellar pocket. Parasites with enlarged flagellar pockets are clearly visible in the DDD85646-treated trypanosome population (Fig. 3e). Additional studies are required to fully understand the cellular effects of NMT inhibition.

Inhibitor acts ‘on-target’

Incubation of BSF *T. brucei* with [^{3}H]-myristic acid results in the biosynthetic radiolabelling of myristoylated substrates, particularly the highly abundant variant surface glycoprotein (VSG) 23. Using this method, but including a detergent lysis step that activates an endogenous phospholipase C to release [^{3}H]-myristate label from the glycosylphosphatidylinositol (GPI) anchor of VSG 24, a number of putative *N*-[^{3}H]-

myristoylated proteins were visualised by SDS-PAGE and fluorography (Fig. 4a, lane 2). The labelling of most of these proteins was eliminated by prior treatment with DDD85646 (Fig. 4a, lane 1). To confirm that most of the proteins labelled with [^{3}H]-myristic acid were indeed *N*-myristoylated, a duplicate gel was treated with 0.2 M NaOH in methanol prior to fluorography to remove base-labile hydroxy- or thio-ester linked [^{3}H]-myristate (Fig. 4a, lanes 3 and 4). Three faint DDD85646-insensitive bands were removed (Fig. 4a, compare lanes 1 and 2 with lanes 3 and 4); these most likely include traces of residual GPI anchored VSG at 55 kDa 24 and thioester-myristoylated GPI-PLC at 42 kDa 25. In order to assess whether DDD85646 specifically inhibited *N*-[^{3}H]-myristoylation, the same cells were labelled in parallel with [^{35}S]-methionine. Pre-treatment of parasites with DD85646 had no effect on [^{35}S]-methionine incorporation into proteins, showing that the compound has no effect on general protein synthesis (Fig. 4a, lanes 5 and 6).

Further evidence that DDD85646 was acting on-target in the trypanosome was obtained by over-expressing *Tb*NMT (5-fold) in a tetracycline-inducible manner; this resulted in an 8-fold reduction in DDD85646 potency against these cells (Fig. 4b).

Another independent approach was taken using one of the few known substrates of *Tb*NMT in *T. brucei, Tb*Arf1. This protein plays a central role in endocytosis and Golgi-lysosome trafficking, where tetracycline-induced expression of a constitutively-active GTP-locked mutant (Q71L) causes rapid cell death in BSF *T. brucei* in an *N*-myristoylation-dependent manner 7. Short-term treatment (5 h) with 10 nM DDD85646 rescued these *Tb*Arf1 Q71L expressing cells from death (Fig. 4c), presumably by preventing *N*-myristoylation of newly produced *Tb*Arf1 Q71L protein. Although the Q71L mutant protein could not be detected by Western blotting, as reported previously 7, nonetheless the inducible expression of the related, but myristoylation blocked, G2A Q71L mutant in the presence of DDD85646 does show that its effect on cell survival was not due to interference with tetracycline-induction of these mutants.

Taken together, these data provide strong evidence that DDD85646 acts to inhibit *Tb*NMT in BSF trypanosomes and that this is directly linked to inhibition of proliferation. These data also provide a potential link between inhibition of *Tb*NMT and disruption of the function of the *Tb*NMT substrate *Tb*Arf1, known to operate in protein trafficking and endocytic processes.

Inhibitor binds in *Tb*NMT peptide pocket

The Target Product Profile for a new drug to combat HAT, as defined by Drugs for Neglected Diseases initiative, requires compounds that are safe and efficacious against both the stage 1 disease, when parasites are present in the blood, lymph and interstitial fluids, and the stage 2 disease, when parasites are also present in the CNS. The DDD85646 compound does not yet meet these criteria and will have to be optimised with respect to selectivity over human NMT and for diffusion into the CNS, while retaining excellent potency against *Tb*NMT and BSF *T. brucei* cells. To achieve these objectives, a detailed understanding of the interaction between DDD85646 and *Tb*NMT is required. Characterisation of the mode of inhibition of the early hits revealed competition with respect to peptide substrate as a likely mode of inhibition for the series. Thus, a shift in IC_{50} from 1 to 4.3 μM for an early hit was seen when the peptide substrate concentration in the assay was increased from 0.5 to 16 μM (Fig. 5a). Surface Plasmon Resonance (SPR) studies confirmed a 1:1 binding stoichiometry of DDD85646 with *Tb*NMT (Fig. 5b) and showed that the binding affinity of the compound was increased in the presence of myristoyl-CoA from 33 nM to 1 nM (data not shown). Accurate determination of binding affinity via SPR also revealed a potential small window of selectivity between *Tb*NMT and human NMT with binding constants of 1 and 14 nM,

respectively. Due to tight binding of this compound (see Supplementary Information, Figure 1), this selectivity was less clear in the biochemical assay which recorded 2 and 4 nM (IC_{50}), respectively. Furthermore, this emerging selectivity is clearly driven by differing off-rates and optimisation around this parameter will not only be important in improving selectivity, but also in sustaining a high residency time of binding to *Tb*NMT. The structure of *Tb*NMT has not been solved to date. However, using *L. major* NMT (*Lm*NMT) as a model system, the binding of DDD85646 into the peptide substrate binding site has been confirmed by X-ray crystallography (Fig. 5c, for stereo view see Supplementary Information, Figure 4). *Lm*NMT has 74% overall sequence identity with *Tb*NMT and 94% identity within the peptide-binding site (see Supplementary Information, Figure 5). The binding mode shows the piperazine interacting with the C-terminal carboxylate of NMT, via a tightly coordinated water molecule as opposed to a direct H-bond. The sulfonamide makes water bridged interactions with the highly conserved residue His219 and to the backbone NH group of Gly397. The geometry of the sulfonamide creates a significant bend in the structure, allowing the pyrazole to fit into a lipophilic pocket where it acts as a hydrogen bond acceptor from Ser330. The binding mode is of particular interest because all but the latter interactions are through water-mediated hydrogen bonds; a mode not readily predicted using computational techniques. Overlaying the structure of *Saccharomyces cerevisiae* NMT in complex with substrate peptide (PDB 1IID) 26 with the *Lm*NMT complex shows that DDD85646 occupies the peptide binding site with the basic piperazine moiety mimicking the N-terminus of the substrate (see Supplementary Information, Figure 6).

Conclusions

We have presented evidence that our model *Tb*NMT inhibitor, DDD85646, kills BSF *T. brucei* by acting on *Tb*NMT *in situ*. The downstream consequences of *Tb*NMT inhibition in the parasite are likely to be multiple, since the enzyme has over 60 putative substrates 6, and this no doubt explains the speed of killing and the dramatic morphological changes observed upon treatment with this compound. The emergence of the ‘BigEye’ phenotype, and the possible link to *Tb*Arf1 activity, suggests that disturbance of endocytosis is one mechanism by which *Tb*NMT inhibitors act in BSF *T. brucei*. Interestingly, knockdown of *Tb*NMT levels in BSF *T. brucei* by RNAi to 16% of wild-type levels, while fatal *in vitro* and *in vivo*, does not lead to the ‘BigEye’ phenotype but rather to the accumulation of vesicles close to the flagellar pocket 27.

It is notable that, despite the small window of selectivity between human NMT and *Tb*NMT, DDD85646 shows promising selectivity at the cellular level. One might speculate that *T. brucei* cells are hyper-sensitive to NMT inhibition because of unique or unusual aspects of their biochemistry and/or cell biology. In this context, the extremely high endocytic rate of BSF *T. brucei* (some 9 times faster than fibroblasts and 2.6 times faster than macrophages), combined with the entire endocytic/exocytic process occurring in the flagellar pocket, is noteworthy 28. The parasite’s requirement for this high endocytic rate relates to its need to remove antibody from the cell surface and to recycle the protective VSG coat 29.

Finally, we may conclude that *Tb*NMT is one of the few *T. brucei* proteins that have been comprehensively validated as a drug target for HAT. The *Tb*NMT inhibitors described meet many requirements for a greatly needed new therapeutic for HAT. Further optimisation of this series towards improved CNS penetration and selectivity is currently underway. In the meantime DDD85646 will serve as an excellent chemical tool for investigation of the biology of protein *N*-myristoylation across a range of organisms.

Supplementary Material

Refer to Web version on PubMed Central for supplementary material.

Acknowledgments

This work was supported by grants from the Wellcome Trust (WT077705, WT083481, WT077503 and WT085622), Scottish Funding Council (HR04013) and by the Translational Biology Theme of SULSA. We thank the European Regional Development Fund and the Wolfson Foundation for grants that provided relevant infrastructure for this work. The Structural Genomics Consortium is a registered charity (number 1097737) that receives funds from the Canadian Institutes for Health Research, the Canadian Foundation for Innovation, Genome Canada through the Ontario Genomics Institute, GlaxoSmithKline, Karolinska Institutet, the Knut and Alice Wallenberg Foundation, the Ontario Innovation Trust, the Ontario Ministry for Research and Innovation, Merck & Co., Inc., the Novartis Research Foundation, the Swedish Agency for Innovation Systems, the Swedish Foundation for Strategic Research and the Wellcome Trust. We would like to thank all members of the Drug Discovery Unit for their expert technical assistance in this study, particularly Bhavya Rao, Iain Collie and Daniel James.

Appendix

Methods Summary

Enzyme activity assays were performed in scintillation proximity format18, with minor modifications. Proliferation assays were performed using resazurin as an indicator of metabolic activity30. *Tb*NMT was immobilised onto sensor chips (NTA) using standard immobilisation protocols and kinetics of binding of compound analysed on Biacore T-100. Details of all standard methods including compound exposure studies and efficacy studies, metabolic labelling, microscopy, and crystallography can be found in the Methods section of online versions. Chemical synthesis details can be found in supplementary materials.

Methods

Determination of exposure in rat after acute oral dosing

Female NMRI mice (25-35 g; Harlan Laboratories; n=3 per dose group) were administered DDD85646 at 10 and 50 mg kg^{-1} orally. The dose solutions were prepared on the day of dosing and vehicle was 5% DMSO in deionised water or 5% DMSO, 40% PEG400 in deionised water respectively. Blood samples (10 μl) were collected from the tail vein of each animal into micronic tubes (Micronic BV) containing deionised water (20 μl) at 0.25, 0.5, 1, 2, 4, 6 and 8 h post-dose and stored at −80°C to await analysis.

Sample extraction of blood was performed by a method based on protein precipitation using acetonitrile and a structural analogue of the analyte of interest as internal standard. Blood extracts were analysed by UPLC/MS/MS using a Quattro Premier XE mass spectrometer (Waters). Calibration curves were constructed in blood to cover at least 3 orders of magnitude (i.e. 1-1000 ng ml^{-1}).

Efficacy studies

DDD85646 was tested in vivo against *Trypanosoma brucei brucei* using a modification of the approach used by Thuita *et al.* 31. In brief, female NMRI mice (25-35 g, Harlan Laboratories; 3-5 per group) were infected intraperitoneally with 1×10^4 bloodstream forms of *T. b. brucei* S427 (221). These bloodstream forms come from a stock of cryopreserved stabilates containing 10% glycerol. The stabilate was suspended in phosphate-saline-glucose to obtain a trypanosome concentration of 5×10^4 ml^{-1}. Each mouse was injected with 0.2 ml. DDD85646 was administered orally from day +3 to day +6 of the experiment and parasitaemia levels monitored up to day +30. Animals with parasitaemia > 10^8 ml^{-1} were

humanely killed as previous studies had shown that animals do not survive a further 24 h 32. The day of euthanisation was recorded.

NMT enzyme assay 18,33

NMT assays were carried out at room temperature in 384-well white optiplates (Perkin Elmer). Each assay was performed in a 40 μl reaction volume containing 30 mM Tris, pH 7.4, 0.5 mM EDTA, 0.5 mM EGTA, 1.25 mM DTT, 0.1% (v/v) Triton X-100, 0.125 μM [^{3}H]-myristoyl-coenzyme A (8 Ci mmol^{-1}), 0.5 μM biotinylated CAP5.5, 5 nM NMT and various concentrations of test compound. The IC_{50} values for *hu*NMT1 and *hu*NMT2 were essentially identical against 80 compounds tested and, for logistical reasons, only *hu*NMT1 was used in later studies.

Test compound (0.4 μl in DMSO) was transferred to all assay plates using a Cartesian Hummingbird (Genomics Solution) before 20 μl of enzyme was added to assay plates. The reaction was initiated with 20 μl of a substrate mix and stopped after 15 min (*hu*NMT1 or 2) or 50 min (*Tb*NMT) with 40 μl of a stop solution containing 0.2 M phosphoric acid, pH 4.0 and 1.5 M $MgCl_2$ and 1 mg ml^{-1} PVT SPA beads (GE Healthcare). All reaction mix additions were carried out using a Thermo Scientific WellMate (Matrix). Plates were sealed and read on a TopCount NXT™ Microplate Scintillation and Luminescence Counter (Perkin Elmer).

ActivityBase from IDBS was used for data processing and analysis. All IC_{50} curve fitting was undertaken using XLFit version 4.2 from IDBS. A 4-parameter logistic dose response curve was utilised using XLFit 4.2 Model 205. All test compound curves had floating top and bottom and pre-fit was used for all 4 parameters.

Compound efficacy and trypanocidal activity in cultured T. brucei parasites

Bloodstream *T. b. brucei* S427 were cultured at 37°C in modified HMI9 medium (56 μM 1-thioglycerol was substituted for 200 μM 2-mercaptoethanol) and quantified using a haemocytometer. For the live/dead assay, cells were analysed using a two colour cell viability assay (Invitrogen) as described previously 7. Routine screening of test compounds against parasites was performed in 96-well plates using a modification 30 of the cell viability assay previously described by Raz *et al.* 34. Cell culture plates were stamped with 1 μl of an appropriate concentration of test compound in DMSO followed by the addition of 200 μl trypanosome culture (10^4 cells ml^{-1}) to each well, except for one column which received media only. MRC5 cells were cultured in Dulbecco's Modified Eagle's Medium, seeded at 2,000 cells per well and allowed to adhere overnight. One microlitre of test compound (10 point dilutions from 50 μM to 2 nM) was added to each well at the start of the assay. Culture plates of *T. brucei* and MRC5 cells were incubated at 37°C in an atmosphere of 5% CO_2 for 69 h, prior to the addition of 20 μl resazurin (final concentration 50 μM). After a further 4 h incubation, fluorescence was measured (excitation 528 nm; emission 590 nm) using a BioTek flx800 plate reader.

SPR analysis

The interaction between NMT and DDD85646 was assessed using a Biacore T100 instrument. Histidine-tagged *Tb*NMT and *hu*NMT1 were immobilised onto a NTA sensor chip (GE Healthcare) to levels of ~ 6000 response units (RU) using standard immobilisation protocols (GE Healthcare). Experiments were carried out at 25°C using HBS-P+ running buffer (GE Healthcare) containing 100 nM myristoyl-coenzyme A. DDD85646 binding was tested by injecting varying concentrations of inhibitor (0.05 nM to 1000 nM) at a flow rate of 30 μl min^{-1}. Different concentrations of DDD85646 were prepared so that the final

Europe PMC Funders Author Manuscripts

Europe PMC Funders Author Manuscripts

DMSO concentration was 0.1%. Kinetic data analysis was performed using Biacore T100 Evaluation Software 2.0.1 and fitted to the standard 1:1 interaction model to give results.

Overexpression of NMT and mutant ARF1 studies

The plasmid vector pM2cN was a gift from David Horn and Sam Alsford (LSHTM, UK). The *T. brucei NMT* open reading frame was amplified from genomic DNA using suitable primers and cloned into the plasmid vector pM2cN. The resulting construct encodes the target protein with an N-terminal myc epitope tag under the control of a tetracycline-inducible T7 promoter. Mid-log phase *T. brucei* BSF 'single marker' (*T7RPOL TETR NEO*) S427 (subsequently termed SM) were electroporated with 10 μg of *Not*I-digested pM2cN-TbNMT using methods described 8. Expression of myc-tagged NMT was induced in stable cell lines by incubating parasites in 1 μg ml^{-1} tetracycline for 24 h. Immunoblotting 8 of parasite lysates was performed using the following primary antibodies: mouse anti-myc (Invitrogen, 1:1000 dilution), rabbit anti-*Tb*NMT (1:500 dilution) and rabbit anti-BiP (gift from Jay Bangs, Department of Medical Microbiology and Immunology, Madison, WI, used at 1:10,000 dilution), mouse anti-alpha-tubulin, TAT1 (gift from Keith Gull, Dunn School, University of Oxford). Parental and NMT overexpressing cell lines (induced with tetracycline for 24 h) were seeded in 24-well plates at 5×10^5 ml^{-1} in triplicate, containing 0-100 nM of DDD85646. Motile cells were counted using a haemocytometer.

Production and transfection of the constructs pM2TbARF1-Q71L and pM2TbARF1-G2AQ71L have been described previously 7. Parental and mutant cell lines were seeded in 10 ml cultures at 5×10^5 ml^{-1}. DDD85646 (10 nM) with or without tetracycline (1 μg ml^{-1}) was added to cultures and flasks incubated at 37°C with 5% CO_2 for 6 h. A set of cultures was set up in which tetracycline was added for 1 h before addition of DDD85646 and incubated for a further 5 h. Treated cells were then analysed using a Live/Dead two colour cell viability assay as described previously 7 and immunoblotted using anti-myc antibody 8.

Transmission electron microscopy

T. brucei cells were harvested by centrifugation at 1,000 x g for 10 min and fixed in 1 pellet volume of 4% paraformaldehyde in 0.1 M piperazine-N,N'-bis(2-ethanesulfonic acid) for 30 min at room temperature. Fixed cells were spun at 13,000 g for 10 min, the supernatant was removed, and the pellet was resuspended in 1% aqueous osmium tetroxide (to fix and stain lipids), dehydrated, and set in Durcupan epoxy resin (Sigma). Sections were cut using a Leica Ultracut UCT system and analyzed using a Philips Tecnai 12 transmission electron microscopy instrument.

Metabolic labelling

Live bloodstream form *T. brucei* (10^7) were incubated with and without 0.5 μM DDU85646 compound in 10 ml HMI-9 for 6 h at 37°C in a 5% CO_2 incubator and subsequently labelled with 50 μCi ml^{-1} [^{3}H]-myristic acid or 20 μCi ml^{-1} [^{35}S]-methionine for 1 h at 37°C. The cells were washed in trypanosome dilution buffer and lysed in 1% TX-100 in 10 mM sodium phosphate buffer, pH 8 and incubated for 10 min at 37°C. Duplicate aliquots of lysates were run in 4-12% Nupage gels, stained with Coomassie blue and subsequently treated, or not, with 0.2 M NaOH in MeOH for 1 h at room temperature. The gels were washed and soaked in En^{3}Hance, dried and exposed to film.

Crystallography

*Lm*NMT protein was obtained from the Structural Genomics Consortium parasitic disease project (courtesy R. Hui, SGC Toronto). The protein construct consisted of 6xHis, TEV

cleavage site, *Lm*NMT 5-421 which was prepared in 10 mM HEPES pH 7.5, 500 mM NaCl at 9 mg/ml for crystallisation. A 200 mM stock solution of DDD85646 was prepared in DMSO and added to the protein solution to a final concentration 10 mM. Myristoyl CoA was also added to sample to a final concentration of 1 mM prior to crystallisation. Crystallisation was carried out using vapour diffusion methods at with 2 μl of protein:ligand complex mixed with 2 μl of reservoir solution. The reservoir solution contained 26% PEG 1500, 0.2 M NaCl, 0.1M Na Cacodylate pH 5.6. X-ray diffraction data for *Lm*NMT + DDD85646 were measured at the European Synchrotron Facility (ESRF, Grenoble, France) at beamline ID14-1. The data were integrated and scaled using the HKL suite 35. The structure was solved by molecular replacement as implemented in MOLREP 36 using the native *Lm*NMT coordinates (PDB 3H5Z) as a search model. The structure was refined using REFMAC5 37 and manual alteration of the model carried out using COOT 38. Ligand coordinates and topology files were created using the PRODRG server 39. Data collection and refinement statistics are presented in Supplementary Table 1.

Reference List

31. Thuita JK, et al. Efficacy of the diamidine DB75 and its prodrug DB289, against murine models of human African trypanosomiasis. Acta Trop. 2008; 108:6–10. [PubMed: 18722336]
32. Sienkiewicz N, Jaroslawski S, Wyllie S, Fairlamb AH. Chemical and genetic validation of dihydrofolate reductase-thymidylate synthase as a drug target in African trypanosomes. Mol. Microbiol. 2008; 69:520–533. [PubMed: 18557814]
33. Bowyer PW, et al. Molecules incorporating a benzothiazole core scaffold inhibit the *N*-myristoyltransferase of *Plasmodium falciparum*. Biochem. J. 2007; 408:173–180. [PubMed: 17714074]
34. Raz B, et al. The Alamar Blue® assay to determine drug sensitivity of African trypanosomes (*T.b.rhodesiense* and *T.b.gambiense*) in vitro. Acta Trop. 1997; 68:139–147. [PubMed: 9386789]
35. Otwinowski Z, Minor W. Processing of X-ray diffraction data collected in oscillation mode. Methods Enzymol. 1997; 276:307–326.
36. Vagin A, Teplyakov A. MOLREP: an automated program for molecular replacement. J. Appl. Cryst. 1997; 30:1022–1025.
37. Murshudov GN, Vagin AA, Dodson EJ. Refinement of macromolecular structures by the maximum-likelihood method. Acta Crystallogr. D. 1997; 53:240–255. [PubMed: 15299926]
38. Emsley P, Cowtan K. *Coot*: model-building tools for molecular graphics. Acta Crystallogr. D. 2004; 60:2126–2132. [PubMed: 15572765]
39. Schuttelkopf AW, van Aalten DMF. PRODRG: a tool for high-throughput crystallography of protein-ligand complexes. Acta Crystallogr. D. 2004; 60:1355–1363. [PubMed: 15272157]

Reference List

1. Farazi TA, Waksman G, Gordon JI. The biology and enzymology of protein *N*-myristoylation. J. Biol. Chem. 2001; 276:39501–39504. [PubMed: 11527981]
2. Resh MD. Trafficking and signaling by fatty-acylated and prenylated proteins. Nat. Chem. Biol. 2006; 2:584–590. [PubMed: 17051234]
3. Maurer-Stroh S, Eisenhaber B, Eisenhaber F. N-terminal *N*-myristoylation of proteins: Prediction of substrate proteins from amino acid sequence. J. Mol. Biol. 2002; 317:541–557. [PubMed: 11955008]
4. Bhatnagar RS, Futterer K, Waksman G, Gordon JI. The structure of myristoyl-CoA : protein *N*-myristoyltransferase. Biochim. Biophys. Acta. 1999; 1441:162–172. [PubMed: 10570244]
5. Price HP, et al. Myristoyl-CoA : protein *N*-myristoyltransferase, an essential enzyme and potential drug target in kinetoplastid parasites. J. Biol. Chem. 2003; 278:7206–7214. [PubMed: 12488459]
6. Mills E, et al. Kinetoplastid PPEF phosphatases: Dual acylated proteins expressed in the endomembrane system of *Leishmania*. Mol. Biochem. Parasitol. 2007; 152:22–34. [PubMed: 17169445]

7. Price HP, Stark M, Smith DF. *Trypanosoma brucei* ARF1 plays a central role in endocytosis and Golgi-lysosome trafficking. Mol. Biol. Cell. 2007; 18:864–873. [PubMed: 17182848]
8. Price HP, Panethymitaki C, Goulding D, Smith DF. Functional analysis of functional analysis of TbARL1, an *N*-myristoylated Golgi protein essential for viability in bloodstream trypanosomes. J. Cell Sci. 2005; 118:831–841. [PubMed: 15687105]
9. Hertz-Fowler C, Ersfeld K, Gull K. CAP5.5, a life-cycle-regulated, cytoskeleton-associated protein is a member of a novel family of calpain-related proteins in *Trypanosoma brucei*. Mol. Biochem. Parasitol. 2001; 116:25–34. [PubMed: 11463463]
10. Denny PW, et al. Acylation-dependent protein export in *Leishmania*. J. Biol. Chem. 2000; 275:11017–11025. [PubMed: 10753904]
11. Wingard JN, et al. Structural insights into membrane targeting by the flagellar calcium-binding protein (FCaBP), a myristoylated and palmitoylated calcium sensor in *Trypanosoma cruzi*. J. Biol. Chem. 2008; 283:23388–23396. [PubMed: 18559337]
12. Selvakumar P, et al. Potential role of *N*-myristoyltransferase in cancer. Progress in Lipid Research. 2007; 46:1–36. [PubMed: 16846646]
13. Georgopapadakou NH. Antifungals targeted to protein modification: focus on protein *N*-myristoyltransferase. Expert Opinion on Investigational Drugs. 2002; 11:1117–1125. [PubMed: 12150705]
14. Hill BT, Skowronski J. Human *N*-myristoyltransferases form stable complexes with lentiviral Nef and other viral and cellular substrate proteins. J. Virol. 2005; 79:1133–1141. [PubMed: 15613341]
15. Bowyer PW, et al. *N*-myristoyltransferase: a prospective drug target for protozoan parasites. ChemMedChem. 2008; 3:402–408. [PubMed: 18324715]
16. Sheng C, et al. Homology modeling and molecular dynamics simulation of *N*-myristoyltransferase from protozoan parasites: active site characterization and insights into rational inhibitor design. J. Comput. Aided Mol. Des. 2009; 23:375–389. [PubMed: 19370313]
17. Giang DG, Cravatt BF. A second mammalian *N*-myristoyltransferase. J. Biol. Chem. 1998; 273:6595–6598. [PubMed: 9506952]
18. Panethymitaki C, et al. Characterization and selective inhibition of myristoyl-CoA : protein *N*-myristoyltransferase from *Trypanosoma brucei* and *Leishmania major*. Biochem. J. 2006; 396:277–285. [PubMed: 16480339]
19. Brenk R, et al. Lessons learnt from assembling screening libraries for drug discovery for neglected diseases. ChemMedChem. 2008; 3:435–444. [PubMed: 18064617]
20. Doering TL, et al. An analog of myristic acid with selective toxicity for African trypanosomes. Science. 1991; 252:1851–1854. [PubMed: 1829548]
21. Allen CL, Goulding D, Field MC. Clathrin-mediated endocytosis is essential in *Trypanosoma brucei*. EMBO J. 2003; 22:4991–5002. [PubMed: 14517238]
22. Hall B, Allen CL, Goulding D, Field MC. Both of the Rab5 subfamily small GTPases of *Trypanosoma brucei* are essential and required for endocytosis. Mol. Biochem. Parasitol. 2004; 138:67–77. [PubMed: 15500917]
23. Ferguson MAJ, Cross GAM. Myristylation of the membrane form of a *Trypanosoma brucei* variant surface glycoprotein. J. Biol. Chem. 1984; 259:3011–3015. [PubMed: 6699005]
24. Ferguson MAJ, Low MG, Cross GAM. Glycosyl-*sn*-1,2-dimyristylphosphatidylinositol is covalently linked to *Trypanosoma brucei* variant surface glycoprotein. J. Biol. Chem. 1985; 260:4547–4555. [PubMed: 3157681]
25. Armah DA, Mensa-Wilmot K. *S*-myristoylation of a glycosylphosphatidylinositol-specific phospholipase C in *Trypanosoma brucei*. J. Biol. Chem. 1999; 274:5931–5938. [PubMed: 10026218]
26. Farazi TA, Waksman G, Gordon JI. Structures of *Saccharomyces cerevisiae N*-myristoyltransferase with bound myristoylCoA and peptide provide insights about substrate recognition and catalysis. Biochemistry. 2001; 40:6335–6343. [PubMed: 11371195]
27. Price HP, Guther ML, Ferguson MA, Smith DF. Myristoyl-CoA:protein *N*-myristoyltransferase depletion in trypanosomes causes avirulence and endocytic defects. Mol Biochem. Parasitol. 2010; 169:55–58. [PubMed: 19782106]

28. Overath P, Engstler M. Endocytosis, membrane recycling and sorting of GPI-anchored proteins: *Trypanosoma brucei* as a model system. Mol. Microbiol. 2004; 53:735–744. [PubMed: 15255888]
29. Engstler M, et al. Hydrodynamic flow-mediated protein sorting on the cell surface of trypanosomes. Cell. 2007; 131:505–515. [PubMed: 17981118]
30. Patterson S, et al. Synthesis and evaluation of 1-(1-(benzo[*b*]thiophen-2-yl)cyclohexyl)piperidine (BTCP) analogues as inhibitors of trypanothione reductase. ChemMedChem. 2009; 4:1341–1353. [PubMed: 19557802]

Europe PMC Funders Author Manuscripts

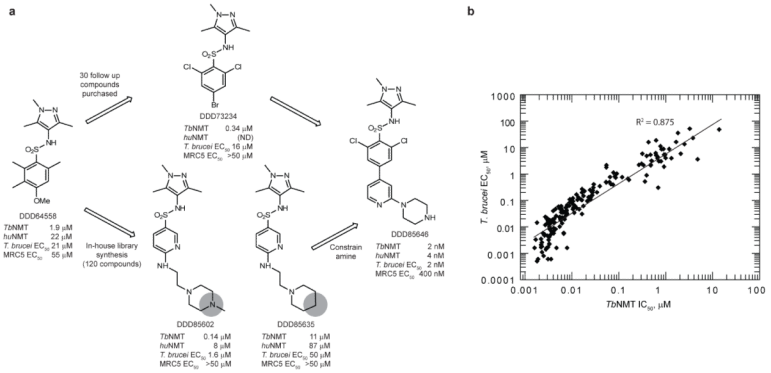

Figure 1. Identification of NMT lead series inhibitors

a. Chemical evolution of DDD85646 from the initial high-throughput screening hit DDD64588. Combining the structure-activity-relationships from the two strategies led to the development of the potent compound DDD85646. Potencies were determined for all compounds synthesised against recombinant *Tb*NMT and *hu*NMT, as well as against BSF *T. brucei* and MRC5 proliferation *in vitro*.

b. Correlation between the inhibitions of recombinant *Tb*NMT and BSF *T. brucei* proliferation for 175 members of the pyrazole sulfonamide series. Data shown are replicates of between 2 and 22 independent potency determinations using 10-point curves. Robustness of *Tb*NMT and trypanosome proliferation assays are exemplified through routinely reported parameters of Z' (0.703 ± 0.050, n=169 and 0.695 ± 0.095, n>1000 for *Tb*NMT and trypanosome assays respectively) and reproducible potencies of standards (DDD73498 (*Tb*NMT assay) pIC_{50} = 6.52 ± 0.14, n=276 and pentamidine (trypanosome assay) pEC_{50} = 8.37 ± 0.41, n=497).

Europe PMC Funders Author Manuscripts

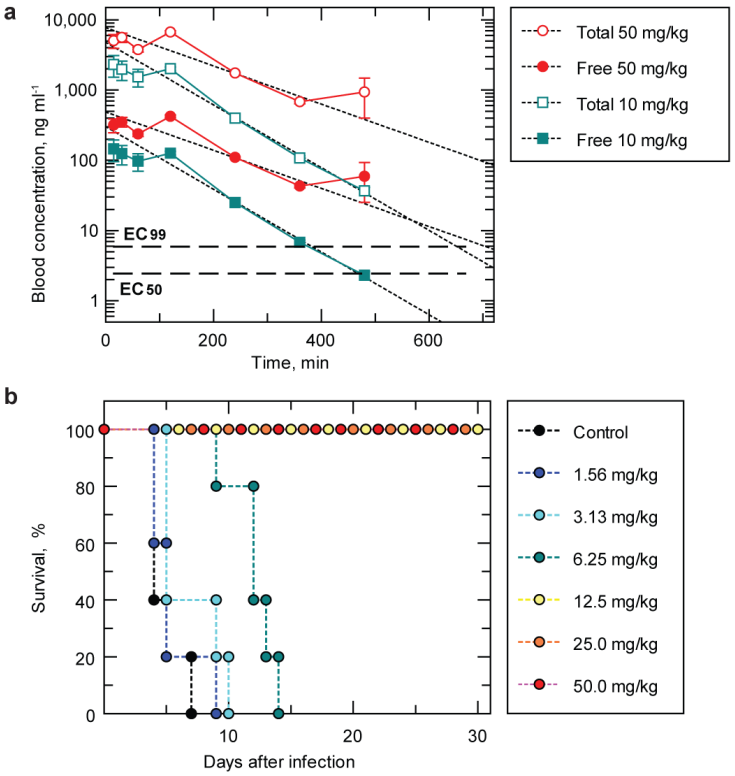

Figure 2. *Tb*NMT inhibitor cures acute trypanosomiasis *in vivo*

a. Mean total and free blood concentration time profiles following single oral administration of DDD85646 at 10 and 50 mg kg^{-1} free base to female NMRI mice (n=3 per dose group). EC_{99} is calculated from the average EC_{50} of 2.46 ± 1.8 nM and Hill slope of 4.84 ± 0.6 (n=5). Solid lines are total plasma concentrations and dashed lines are the predicted free plasma concentrations (fraction unbound in plasma = 0.063).

b. Kaplan Meier survival plot for female NMRI mice (n=5 per dose group) following infection with *T. b. brucei* strain 427 (variant 221) (inoculum 1×10^4 parasites). Oral treatment with DDD85646 commenced 3 days after infection at the indicated doses (all b.i.d for 4 days).

Europe PMC Funders Author Manuscripts

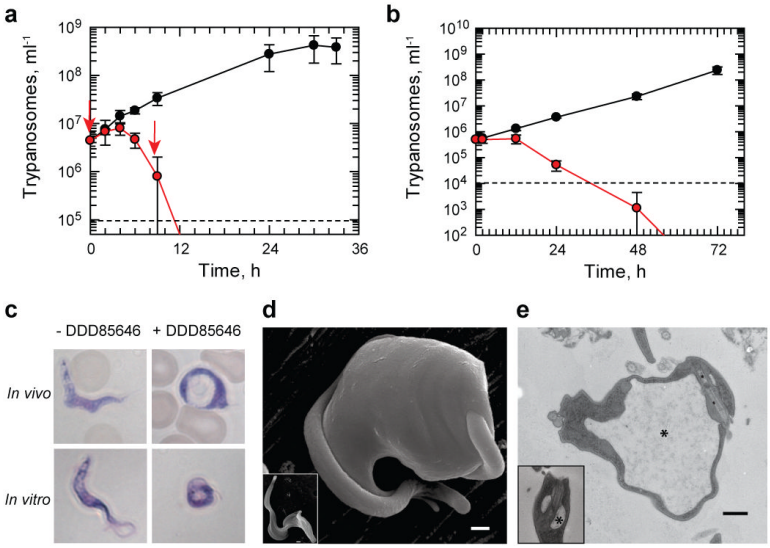

Figure 3. *Tb*NMT inhibitors have rapid trypanocidal effects *in vitro* and *in vivo*

a. Parasitaemia in mice (n=3 per group) with (red) or without (black) DDD85646 treatment (50 mg kg^{-1}, oral, b.i.d); for method see Figure 2b. Arrows represent dose administration times. Data: mean ± s.d.

b. *T. b. brucei* proliferation in culture determined by counting motile parasites in presence (red) or absence (black) of 50 nM DDD85646. Data: mean ± s.d. for 3 determinations.

c. Blood smears of infected mice and culture samples were stained by Giemsa and observed by light microscopy. Treated cells showed typical BigEye phenotype.

d. Scanning electron micrograph of *T. b. brucei* treated with 10 nM DDD85646 for 24 h. Inset shows an untreated control cell.

e. Transmission electron micrograph of sagittal section of flagellar pocket of *T. b. brucei* treated with 5 nM DDD85646 for 72 h. Inset shows a section of flagellar pocket of an untreated control cell.

Asterisks mark flagellar pockets. Dashed lines: cell detection limits. Scale bars: 500 nm.

Europe PMC Funders Author Manuscripts

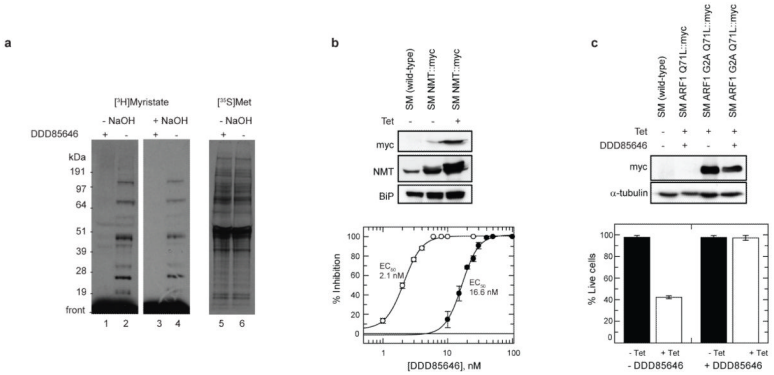

Figure 4. Pyrazole sulfonamide series acts 'on-target' in the trypanosome

a. Fluorographs of SDS-PAGE gels loaded with lysates of BSF *T. b. brucei* cells labelled with either [^{3}H]-myristic acid (lanes 1-4) or [^{35}S]-methionine (lanes 5 and 6) after pre-incubation with (+) or without (−) 0.5 μM DDD85646 for 6 h. Gels were incubated with or without 0.2 M NaOH in methanol, as indicated, prior to fluorography.

b. Wild-type ("single marker", SM) parasites and *T. b. brucei* over-expressing myc-tagged NMT were incubated with 0-100 nM DDD85646 for 64 h; motile cells were counted using a haemocytometer. Closed circles, *T. brucei* over-expressing NMT (n=3); open circles, wild-type cells (n=3). Levels of myc-tagged NMT expression were confirmed via western blotting.

c. *T. b. brucei* expressing ARF1Q71L (GTP-locked form of ARF1) under tetracycline control were treated with 10 nM DDD85646 for 6 h. Cells were then subjected to live/dead FACS analysis. Data shown represent mean ± s.d. from 2 independent experiments. Levels of myc-tagged ARF1 mutant expression were analysed via western blotting.

Europe PMC Funders Author Manuscripts

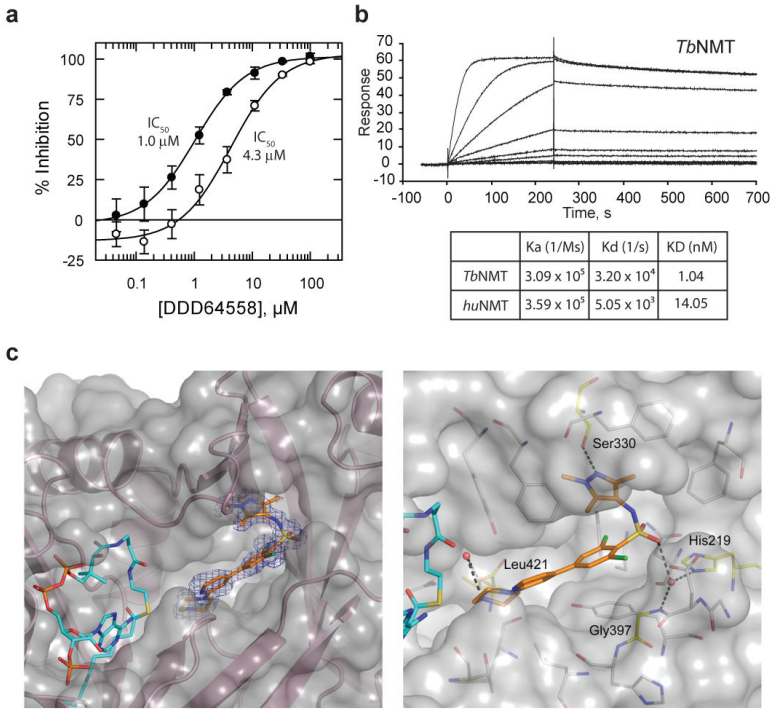

Figure 5. Characterisation of pyrazole sulfonamide interactions with NMT

a, DDD64558 potency against *Tb*NMT (IC_{50}) determined in the presence of 0.5 (closed circles) and 16 µM (open circles) CAP5.5 peptide substrate. Each data point represents mean ± s.d. (n=4).

b, Kinetics of binding of DDD85646 to *Tb*NMT and *hu*NMT1 determined by SPR.

c, X-ray crystal structure of DDD85646 bound to *Lm*NMT. Left panel shows the *Lm*NMT binding site with protein backbone (pink ribbon), solvent accessible surface (grey), DDD85646 (stick representation, carbon atoms gold, nitrogen blue, chlorine green, oxygen red and sulphur yellow), myristoyl CoA (C atoms cyan) and an omit map (F_o-F_c, 3.0 sigma) around DDD85646 (blue). Right panel shows in stick representation DDD85646 and residues forming the active site (C atoms grey). Key residues are highlighted (C atoms yellow) as are water molecules (red spheres) and H-bonds (dashed lines).

Europe PMC Funders Author Manuscripts